Journal of Magnetic Resonance 206 (2010) 127–133

Contents lists available at ScienceDirect

Journal of Magnetic Resonance

journal homepage: www.elsevier.com/locate/jmr

# Density matrix tomography of singlet states

Soumya Singha Roy, T.S. Mahesh *

*NMR Research Center, Indian Institute of Science Education and Research, Pune 411 008, India*

ARTICLE INFO

*Article history:*
Received 5 May 2010
Revised 11 June 2010
Available online 30 June 2010

*Keywords:*
Singlet states
Long-lived states
Quantum state tomography
Density matrix tomography

ABSTRACT

First direct and quantitative study of singlet states using density matrix tomography is reported. A robust scheme for the tomography of a general density matrix of two spin 1/2 nuclei is introduced for this purpose. The study is carried out at different spin-lock conditions and the results are compared.



## 1. Introduction

The long lifetimes of nuclear spin coherences enable NMR spectroscopists to carry out a variety of spin choreography [1,2]. Nuclear spin coherences decay though over time mainly due to spin-spin relaxation and magnetic field inhomogeneity. Often coherences are converted into longitudinal nuclear spin orders to study slow processes. But even the longitudinal spin orders decay toward equilibrium state due to spin-lattice relaxation. Hence for a typical NMR experiment consisting of preparing and measuring certain correlated spin states, the ultimate time barrier was assumed to be defined by the spin-lattice relaxation time constant $T_1$ [3].

It has recently been demonstrated that there exist certain 'long-lived states' which decay slower than the $T_1$ values of individual spins [4–11]. This way, overcoming the $T_1$ barrier has led to several exciting applications in studying slow molecular dynamics and transport processes [12,13], precise measurements of NMR interactions [14], and the transport and storage of hyperpolarized nuclear spin order [15–20].

In a pair of magnetically equivalent nuclei, the singlet state $|S_0\rangle = (|01\rangle - |10\rangle)/\sqrt{2}$, and the triplet states $|T_1\rangle = |00\rangle, |T_0\rangle = (|01\rangle + |10\rangle)/\sqrt{2}$, and $|T_{-1}\rangle = |11\rangle$ form an orthonormal eigenbasis of the internal Hamiltonian $\mathscr{H}_J = I^1 \cdot I^2$. Here $I^k$ are the spin angular momentum operators, and $\{|00\rangle, |01\rangle, |10\rangle, |11\rangle\}$ are the eigenstates of $I_z^1 + I_z^2$ operator. Levitt and co-workers observed that the singlet state $|S_0\rangle$ is a long-lived state [4,5]. Though several molecules such as $H_2$, $H_2O$, etc. satisfy the magnetic equivalence criterion, they are not relevant here since the singlet states by themselves are inaccessible to macroscopic observables. To access the singlet state, the equivalence has to be broken, and the singlet magnetization has to be converted into an observable single quantum coherence. Levitt and co-workers have prepared long-lived singlet states by imposing the equivalence on asymmetric systems and converted them into observable single quantum coherences after releasing the imposed equivalence [4,5]. The equivalence can be imposed either by vanishing the Zeeman field [4] or by using an RF spin-lock [5]. Bodenhausen and co-workers have demonstrated that the singlet spin-lock can also be achieved by RF modulations which are used in heteronuclear spin-decoupling [21]. Detailed theoretical analysis of zero-field singlet states as well as singlet spin-lock have already been provided by Levitt and co-workers [6,22] and by Karthik and Bodenhausen [7]. Recently, long-lived states in multiple-spin systems are also being explored [15,23].

Previously the singlet states were detected indirectly by converting them into detectable antiphase magnetization [4,5]. In this work, we have carried out complete density matrix tomography of singlet states. Tomography enables us not only to quantify the singlet content in a given experimental setting, but also to capture the detailed spin dynamics during the spin-lock period. In the following section we describe a robust density matrix tomography scheme which is particularly suited to study homonuclear systems with small chemical shift differences. In the later sections we explain the experimental setup and characterization of the singlet state tomography.

## 2. Density matrix tomography

Density matrix tomography enables us to measure all elements of a general density matrix. Earlier schemes of tomography were designed in the context of quantum information processing [24,25]. They required spin-selective rotations and transition selective integrations of spectra. In homonuclear spin systems, particu-

* Corresponding author.
*E-mail address:* mahesh.ts@iiserpune.ac.in (T.S. Mahesh).

1090-7807/$ - see front matter © 2010 Elsevier Inc. All rights reserved.
doi:10.1016/j.jmr.2010.06.014

larly in $^1$H spin systems, it is hard to design high fidelity spin-selective rotations owing to the small differences in chemical shifts (on the other hand, the heteronuclear singlet state is predicted to be short-lived [22]). These spin selective pulses generally tend to be long in duration, still introduce significant errors. Integration of individual transitions is also problematic since the transitions, particularly those with mixed line shapes corresponding to a general density matrix, may severely overlap. Tomography based on two-dimensional NMR spectroscopy had also been proposed [26]. This is a general method in the sense only one 2D experiment is needed to be carried out irrespective of the size of the spin system. However, the 2D method is time consuming. Also since it relies on fitting the 2D cross-sections (along the indirect dimension) to mixed Lorentzians, the accuracy is limited by the quality of the fit that is achieved. In the following we present a robust density matrix tomography for a homonuclear weakly coupled two spins-1/2 system which needs only non-selective RF pulses and integrations over each spin instead of individual transitions.

The general traceless deviation density matrix consists of 15 independent real numbers:

$$\rho = \begin{pmatrix} p_0 & r_3 + is_3 & r_1 + is_1 & r_5 + is_5 \\ & p_1 & r_6 + is_6 & r_2 + is_2 \\ & & p_2 & r_4 + is_4 \\ & & & -\sum_{i=0}^{2} p_i \end{pmatrix}. \quad (1)$$

Here real elements $p_k$ are populations and the complex elements $r_k + i\, s_k$ correspond to single ($k$ = 1–4), double ($k$ = 5), and zero ($k$ = 6) quantum coherences. The elements below the diagonal are determined by the Hermitian condition $\rho_{jk} = \rho^*_{kj}$. Since only single quantum coherences are directly observable, four combinations $R_1 := (r_1 + r_2)$, $S_1 := (s_1 + s_2)$, $R_2 := (r_3 + r_4)$, and $S_2 := (s_3 + s_4)$ can be obtained from the integration of complex line shapes of spins 1 and 2 respectively. Now consider an RF sequence with propagator $U$, that transforms the original density matrix $\rho$ into $\rho' = U\rho U^\dagger$. Single quantum coherences of $\rho'$ will lead to different linear combinations of various elements in $\rho$. Thus, by applying different propagators on $\rho$, we can measure the values of different linear combinations of various elements of $\rho$. The real and imaginary values of the integration of $j$th spin in $k$th experiment will be labeled as $R_j^k$ and $S_j^k$ respectively. Following six one-dimensional NMR experiments were found to be sufficient to tomograph a two-spin density matrix:

1. $\mathbb{1}$
2. $90_x$
3. $\frac{1}{4J} \cdot 180_x \cdot \frac{1}{4J}$
4. $45_x \frac{1}{4J} \cdot 180_x \cdot \frac{1}{4J}$
5. $45_y \frac{1}{4J} \cdot 180_x \cdot \frac{1}{4J}$
6. $\frac{1}{2\Delta\nu} \cdot 45_y \frac{1}{4J} \cdot 180_x \cdot \frac{1}{4J}$

Here $\mathbb{1}$ is the identity i.e., direct observation without applying any extra pulses. $\Delta\nu$ and $J$ are the chemical shift difference and the scalar coupling respectively (both in Hz). The offset is assumed to be at the center of the two doublets and the RF amplitudes are assumed to be much stronger than $\Delta\nu$. By calculating the propagator for each of these experiments, following set of linear equations were obtained:

$$\begin{bmatrix}
0 & 0 & 0 & 1 & 1 & 0 & 0 & 0 & 0 & 0 & 0 & 0 & 0 & 0 & 0 \\
0 & 0 & 0 & 0 & 0 & 1 & 1 & 0 & 0 & 0 & 0 & 0 & 0 & 0 & 0 \\
0 & 0 & 0 & 0 & 0 & 0 & 0 & 0 & 0 & 1 & 1 & 0 & 0 & 0 & 0 \\
0 & 0 & 0 & 0 & 0 & 0 & 0 & 0 & 0 & 0 & 0 & 1 & 1 & 0 & 0 \\
0 & 0 & 0 & 1 & 1 & 0 & 0 & 0 & 0 & 0 & 0 & 0 & 0 & 0 & 0 \\
0 & 0 & 0 & 0 & 0 & 1 & 1 & 0 & 0 & 0 & 0 & 0 & 0 & 0 & 0 \\
\frac{1}{2} & \frac{1}{2} & \frac{-1}{2} & 0 & 0 & 0 & 0 & 0 & 0 & 0 & 0 & 0 & 0 & 0 & 0 \\
\frac{1}{2} & \frac{-1}{2} & \frac{1}{2} & 0 & 0 & 0 & 0 & 0 & 0 & 0 & 0 & 0 & 0 & 0 & 0 \\
0 & 0 & 0 & 0 & 0 & 0 & 0 & 0 & 0 & 1 & -1 & 0 & 0 & 0 & 0 \\
0 & 0 & 0 & 0 & 0 & 0 & 0 & 0 & 0 & 0 & 0 & 1 & -1 & 0 & 0 \\
0 & 0 & 0 & 1 & -1 & 0 & 0 & 0 & 0 & 0 & 0 & 0 & 0 & 0 & 0 \\
0 & 0 & 0 & 0 & 0 & 1 & -1 & 0 & 0 & 0 & 0 & 0 & 0 & 0 & 0 \\
\frac{1}{4} & \frac{-1}{4} & \frac{-1}{4} & 0 & 0 & 0 & 0 & \frac{1}{2} & \frac{-1}{2} & \frac{1}{2} & \frac{-1}{2} & \frac{-1}{2} & \frac{1}{2} & 0 & 0 \\
\frac{1}{4} & \frac{-1}{4} & \frac{-1}{4} & 0 & 0 & 0 & 0 & \frac{1}{2} & \frac{-1}{2} & \frac{-1}{2} & \frac{1}{2} & \frac{1}{2} & \frac{-1}{2} & 0 & 0 \\
0 & 0 & 0 & \frac{1}{\sqrt{2}} & \frac{-1}{\sqrt{2}} & 0 & 0 & 0 & 0 & 0 & 0 & 0 & 0 & \frac{-1}{\sqrt{2}} & \frac{1}{\sqrt{2}} \\
0 & 0 & 0 & 0 & 0 & \frac{1}{\sqrt{2}} & \frac{-1}{\sqrt{2}} & 0 & 0 & 0 & 0 & 0 & 0 & \frac{-1}{\sqrt{2}} & \frac{-1}{\sqrt{2}} \\
0 & 0 & 0 & 0 & 0 & 0 & 0 & 0 & 0 & \frac{1}{\sqrt{2}} & \frac{-1}{\sqrt{2}} & 0 & 0 & \frac{-1}{\sqrt{2}} & \frac{-1}{\sqrt{2}} \\
0 & 0 & 0 & 0 & 0 & 0 & 0 & 0 & 0 & 0 & 0 & \frac{1}{\sqrt{2}} & \frac{-1}{\sqrt{2}} & \frac{-1}{\sqrt{2}} & \frac{1}{\sqrt{2}} \\
\frac{1}{4} & \frac{-1}{4} & \frac{-1}{4} & \frac{1}{2} & \frac{-1}{2} & \frac{-1}{2} & \frac{1}{2} & \frac{-1}{2} & \frac{-1}{2} & 0 & 0 & 0 & 0 & 0 & 0 \\
\frac{1}{4} & \frac{-1}{4} & \frac{-1}{4} & \frac{-1}{2} & \frac{1}{2} & \frac{1}{2} & \frac{-1}{2} & \frac{-1}{2} & \frac{-1}{2} & 0 & 0 & 0 & 0 & 0 & 0 \\
\frac{1}{4} & \frac{-1}{4} & \frac{-1}{4} & \frac{1}{2} & \frac{-1}{2} & \frac{1}{2} & \frac{-1}{2} & \frac{1}{2} & \frac{1}{2} & 0 & 0 & 0 & 0 & 0 & 0 \\
\frac{1}{4} & \frac{-1}{4} & \frac{-1}{4} & \frac{-1}{2} & \frac{1}{2} & \frac{-1}{2} & \frac{1}{2} & \frac{1}{2} & \frac{1}{2} & 0 & 0 & 0 & 0 & 0 & 0 \\
0 & 0 & 0 & 0 & 0 & 0 & 0 & 0 & 0 & \frac{-1}{\sqrt{2}} & \frac{1}{\sqrt{2}} & 0 & 0 & \frac{-1}{\sqrt{2}} & \frac{-1}{\sqrt{2}} \\
0 & 0 & 0 & 0 & 0 & 0 & 0 & 0 & 0 & 0 & 0 & \frac{1}{\sqrt{2}} & \frac{-1}{\sqrt{2}} & \frac{-1}{\sqrt{2}} & \frac{1}{\sqrt{2}}
\end{bmatrix}
\begin{bmatrix} p_0 \\ p_1 \\ p_2 \\ r_1 \\ r_2 \\ r_3 \\ r_4 \\ r_5 \\ r_6 \\ s_1 \\ s_2 \\ s_3 \\ s_4 \\ s_5 \\ s_6 \end{bmatrix}
=
\begin{bmatrix}
R_1^1 \\ R_2^1 \\ S_1^1 \\ S_2^1 \\ R_1^2 \\ R_2^2 \\ S_1^2 \\ S_2^2 \\ R_1^3 \\ R_2^3 \\ S_1^3 \\ S_2^3 \\ R_1^4 \\ R_2^4 \\ S_1^4 \\ S_2^4 \\ R_1^5 \\ R_2^5 \\ S_1^5 \\ S_2^5 \\ R_1^6 \\ R_2^6 \\ S_1^6 \\ S_2^6
\end{bmatrix}. \quad (2)$$

Certainly, this is a over-determined problem since 24 linear equations are to be used for 15 unknowns. This redundancy however works to increase the precision of the solution by reducing the condition number of the constraint matrix [27]. For the $24 \times 15$ matrix in Eq. (2), condition number is about 3.7, meaning the solutions are precise to five significant digits. The Eq. (2) can be solved either by singular value decomposition or by Gaussian elimination method (both of which are implemented in MATLAB). It may be possible to take into account of $T_2$ decay during the $1/2J$ delays and of strong coupling effects by suitably modifying the constraint matrix. These extensions are skipped for the sake of simplicity.

## 3. Experimental setup

Two $^1$H spins of 5-bromothiophene-2-carbaldehyde were used to study singlet state (Fig. 1). The sample was dissolved in dimethyl sulphoxide-D6 and all the experiments are carried out in Bruker 500 MHz NMR spectrometer at 300 K. The difference $\Delta\nu$ in chemical shifts is 192.04 Hz and the scalar coupling $J$ is 4.02 Hz. Scalar coupling to aldehyde proton was too weak to be observed. The spin lattice relaxation time constants ($T_1$) for the two spins obtained from inversion recovery experiment are 5.2 s and 6.2 s respectively for the spins 1 and 2.

## 4. Singlet state characterization

### 4.1. Observing through antiphase magnetization

The singlet state was prepared by the RF spin-lock method and converted into antiphase magnetizations as described by Carravetta and Levitt [5] using the pulse sequence shown in Fig. 2a. The RF spin-lock was achieved by either CW irradiation or by WALTZ-16 modulations. The RF offset was set to the center of the two chemical shifts in these experiments. The total magnitude of the antiphase magnetizations decays at different rates depending on the spin-lock conditions (Figs. 3 and 4). The decay constants with CW spin-lock are 16.6 s (Fig. 3a) and 13.4 s (Fig. 3h) respectively at RF amplitudes of 2 kHz and 500 Hz. Under WALTZ-16 spin-lock, the decay constants are slightly smaller, 16.2 s (Fig. 4a) and 12.8 s (Fig. 4h) respectively at 2 kHz and 500 Hz. Nevertheless, these values are about 2–3 times the $T_1$ values of the individual spins implying the preparation of long-lived singlet state.

In this scheme, the integrated magnitude spectrum is usually monitored as a function of spin-lock time. The contributions from the spurious coherences may not be eliminated in this process. Further, the double quantum coherences, if any, are not observed at all. Our interest is to quantify the singlet content in the instantaneous state $\rho(t)$ during the spin-lock. One might guess that the singlet content is maximum in the beginning and exponentially

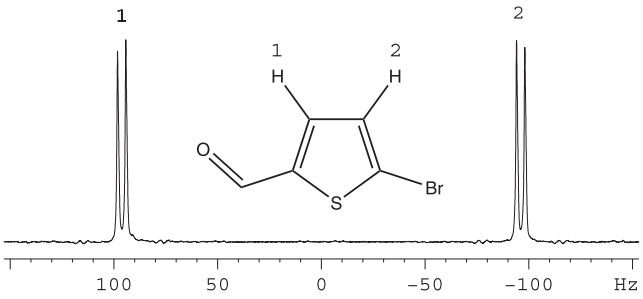


**Fig. 1.** Part of the $^1$H spectrum of 5-bromothiophene-2-carbaldehyde (inset), displaying the doublets corresponding to the two $^1$H spins used to study the singlet state.

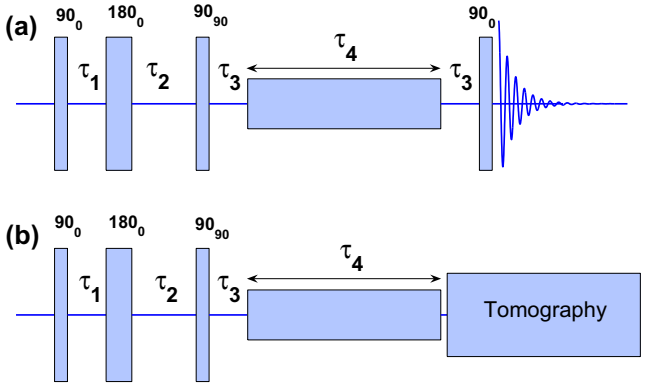


**Fig. 2.** The pulse sequences for the preparation of singlet states and detection via (a) converting to antiphase single quantum magnetization and (b) tomography of singlet states. Here $\tau_1 = 1/(4J)$, $\tau_2 = 1/(4J) + 1/(2\Delta\nu)$, and $\tau_3 = 1/(4\Delta\nu)$, with $\Delta\nu$ and $J$ being the chemical shift difference (in Hz) and the scalar coupling respectively. $\tau_4$ is the duration of spin-lock.

decays with the spin-lock time. Further, one may also guess that CW spin-lock is superior to WALTZ-16 spin-lock at all timescales. But the following tomography results provide a different picture.

### 4.2. Tomography under varying spin-lock duration

The pulse sequence for the tomography of singlet states is shown in Fig. 2b. The density matrix of the singlet state is $|S_0\rangle\langle S_0| = \frac{1}{4}\mathbb{1} + \rho_s$, with the traceless part $\rho_s = -I_1 \cdot I_2$ being the product of spin angular momentum operators of spins 1 and 2. The correlation of the theoretical singlet state operator $\rho_s$ in the instantaneous experimental density matrix $\rho(t)$ (obtained from tomography),

$$\langle\rho_s\rangle(t) = \frac{\mathrm{trace}[\rho(t)\cdot\rho_s]}{\sqrt{\mathrm{trace}[\rho(t)^2]\cdot\mathrm{trace}[\rho_s^2]}}, \tag{3}$$

gives a measure of singlet content in $\rho(t)$. The normalization used in the above expression disregards the attenuation of $\rho(t)$ itself. Similar definitions can be applied to calculate the correlations $\langle I_x^1\rangle$, $\langle|T_0\rangle\langle T_0|\rangle$, etc. We monitored the correlations as a function of spin-lock time $\tau_4$ from 0 s to 30 s in steps of 0.5 s under different spin-lock conditions using the sequence shown in Fig. 2b. The results are shown in Figs. 3 and 4. 3D bar plots of full density matrices at two particular spin-lock conditions are shown in Fig. 5.

The Figs. 3b, 3i, 4b, and 4i indicate correlation $\langle\rho_s\rangle$ as a function of spin-lock time under various spin-lock conditions. In all the cases, the initial correlation is about 0.8. This is expected, since the initial state prepared by the pulse sequences in Fig. 2 just before the spin-lock is actually

$$\rho(0) = |S_0\rangle\langle S_0| - |T_0\rangle\langle T_0|. \tag{4}$$

With CW spin-lock at a high RF amplitude of 2 kHz (Fig. 3b–g), the singlet correlation $\langle\rho_s\rangle$ quickly reaches to 0.95 in 0.5 s of spin-lock time (Fig. 3b). Most of the spurious coherences and the residual longitudinal magnetizations created during the preparation are destroyed by the RF inhomogeneity during spin-lock. Fig. 3g and n reveal that the initial correlation $\langle|T_0\rangle\langle T_0|\rangle(0)$ is $-0.7 \sim -1/\sqrt{2}$ which is just expected. Within 0.5 s, the $|T_0\rangle\langle T_0|$ content is rapidly reduced. But complete equilibration of triplet levels takes about 5 s. Interestingly, there is a sudden build-up and gradual fall of double quantum coherence as seen in Fig. 3f and m. As the singlet state gets purified, $\langle\rho_s\rangle$ exceeds 0.99 in 6 s and reaches a maximum value of 0.994 at 9.5 s. After about 18 s, $\langle\rho_s\rangle$ starts decaying below 0.99, probably due to the gradual conversion of singlet state to other magnetization modes via the triplet states by relaxation

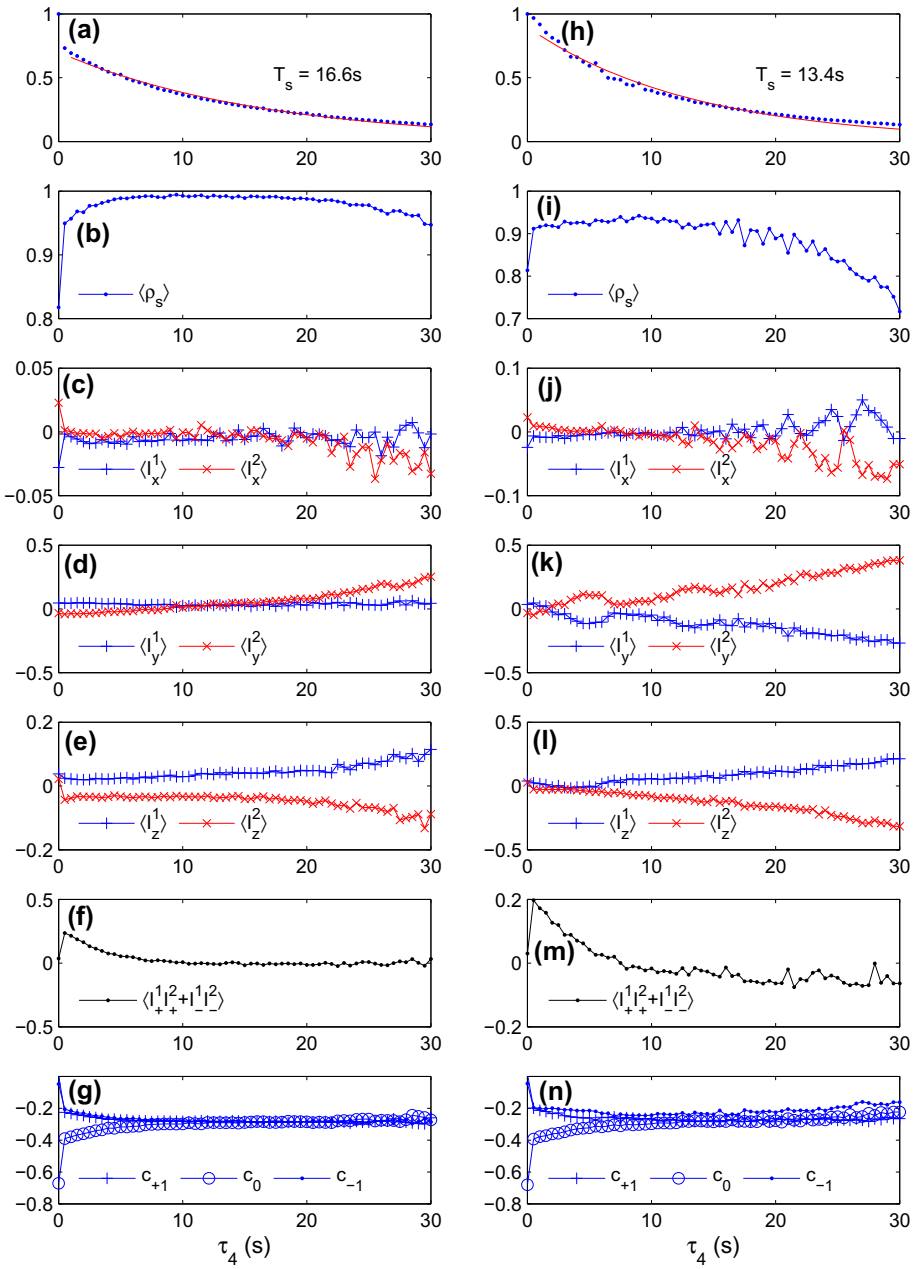


**Fig. 3.** Data characterizing the singlet state under CW spin-lock at an RF amplitude of 2 kHz (a–g) and of 500 Hz (h–n). The spin-lock duration $\tau_4$ was varied from 0 s to 30 s in steps of 0.5 s in each case. Dots in (a) and (h) correspond to the total magnitude of antiphase magnetization obtained from the pulse sequence in Fig. 2a. Singlet decay constant $T_s$ was obtained by using an exponential fit (smooth lines in (a) and (h)). During each fit, first two data points were omitted in view of strong spurious coherences created by the imperfections in the pulses. Remaining graphs are the results obtained from tomography using the pulse sequence shown in Fig. 2b. They correspond to the correlations: $\langle \rho_s \rangle$ (b and i), $\langle I_x^p \rangle$ (c and j), $\langle I_y^p \rangle$ (d and k), $\langle I_z^p \rangle$ (e and l), $\langle I_+^1 I_+^2 + I_-^1 I_-^2 \rangle$ (f and m), and $c_q = \langle |T_q\rangle\langle T_q| \rangle$ (g and n), with spin numbers $p = \{1,2\}$ and triplet subscripts $q = \{-1,0,+1\}$.

mechanisms. On the other hand, there is a gradual build up of *y*- and *z*-magnetizations (Fig. 3d and e) in a similar way as that of a steady state experiment [3,28]. Nevertheless, the singlet correlation remained above 0.95 till 30 s. The x-magnetization and the double quantum coherence (Fig. 3c and f) remained small during the period of high correlation. After the initial differences, the triplet states equilibrate in about 6 s, and remain steady then onwards (Fig. 3g and n).

With CW spin-lock at 500 Hz, the singlet correlation reaches only up to 0.94 again at about 9 s and then steadily drops to 0.71 at 30 s (Fig. 3i). The increased build up of *x*-, *y*-, and *z*-magnetizations with the reduction of the spin-lock power can also be noticed (Fig. 3j-l).

Under WALTZ-16 spin-lock (Fig. 4), all the graphs are characterized by oscillations that are either in-phase or anti-phase. The origin of oscillations probably lies in the cyclic nature of WALTZ-16 modulation.

At an RF amplitude of 2 kHz, the maximum singlet correlation of 0.997 was reached at 15 s (Fig. 4b). The 3D bar plot of the density matrix corresponding to this case is shown in Fig. 5b. More interestingly, $\langle \rho_s \rangle$ peaks seem to maintain above 0.99 till $\tau_4 = 28.5$ s, i.e., about 10 s longer than the CW case! Thus, for certain values of spin-lock durations, WALTZ-16 provides purer singlet states than that of CW.

The singlet correlation under WALTZ-16 spin-lock at 500 Hz displays stronger oscillations (Fig. 4i). Despite the oscillations,

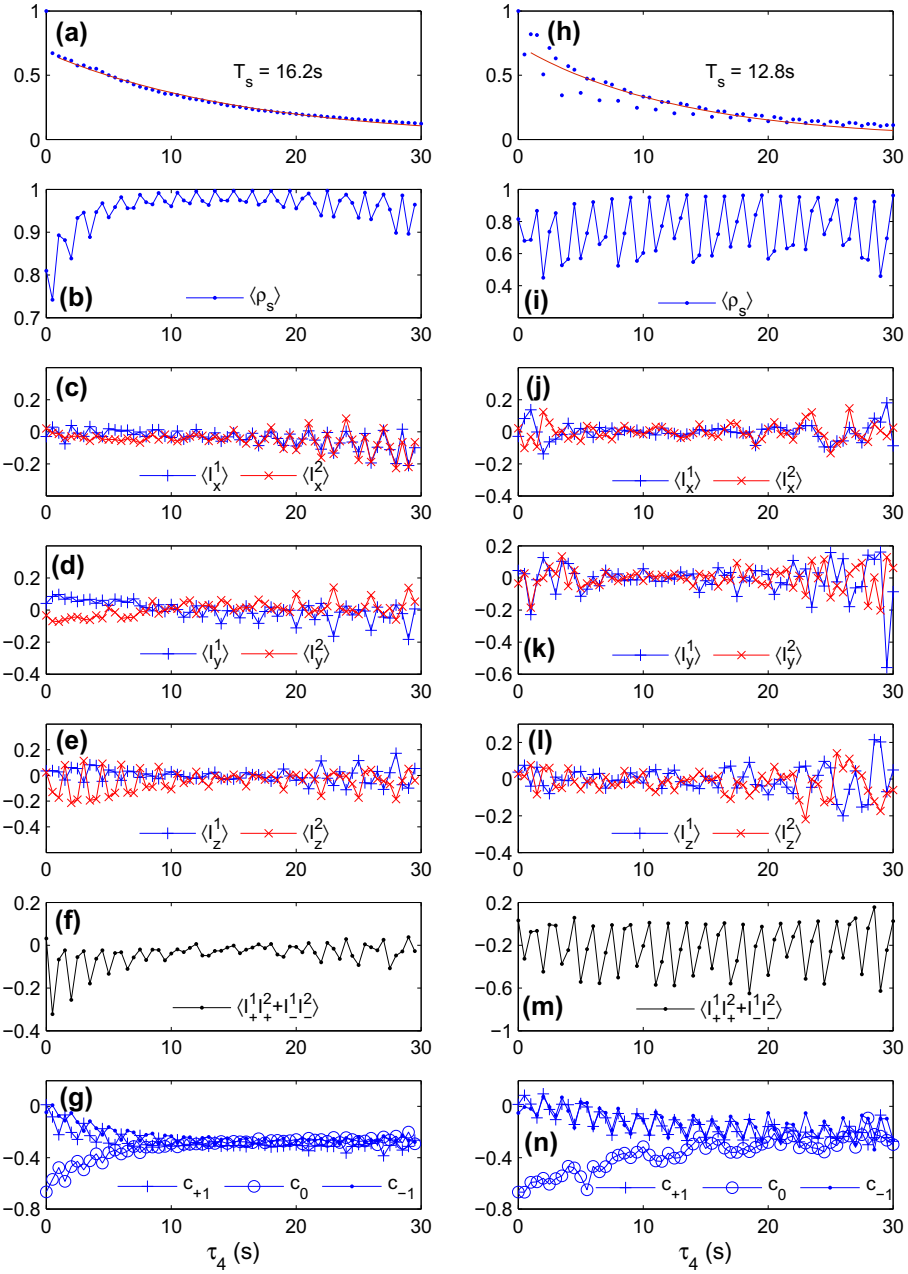


**Fig. 4.** Similar data as in Fig. 3, but under WALTZ-16 spin-lock at an RF amplitude of 2 kHz (a–g) and of 500 Hz (h–n). The graphs correspond to total magnitude of antiphase magnetization (a and h), $\langle \rho_s \rangle$ (b and i), $\langle I^p_x \rangle$ (c and j), $\langle I^p_y \rangle$ (d and k), $\langle I^p_z \rangle$ (e and l), $\langle I^1_+ I^2_+ + I^1_- I^2_- \rangle$ (f and m), and $c_q = \langle |T_q\rangle\langle T_q| \rangle$ (g and n), with spin numbers $p = \{1,2\}$ and triplet subscripts $q = \{-1,0,+1\}$.

the singlet correlation reaches as high as 0.96 at 13.5 s. Again it can be noticed that good singlet content is held for longer periods by WALTZ-16 than the CW of same amplitude. For example at 500 Hz RF amplitude, WALTZ-16 gives a singlet correlation of 0.94 at $\tau_4 = 27$ s, while that for CW it is only 0.79.

### 4.3. Offset dependence

Theoretical and numerical investigations on the offset dependence of singlet spin-lock have been carried out by Karthik and Bodenhausen [7] and by Pileio and Levitt [22]. Robustness of various modulation schemes with regard to offset of singlet spin-lock have been demonstrated by Bodenhausen and co-workers [21]. Here we probe the offset dependence of singlet evolution using tomography.

Fig. 6 shows the experimental data obtained from a series of singlet state tomography experiments, each time varying the RF offset of the spin-lock. The RF offset was measured from the center of the two chemical shifts. Again the experiments were carried out under the following spin-lock conditions: (i) CW for 15 s (Fig. 6a–f), (ii) CW for 28.5 s (Fig. 6g–l), (iii) WALTZ-16 for 15 s (Fig. 6m–r), and (iv) WALTZ-16 for 28.5 s (Fig. 6s–x). The graphs indicate that the WALTZ-16 scheme is far superior compared to CW in preserving the singlet correlation at high RF offsets. The singlet correlations with 2 kHz CW drops below 0.5 for an offset of 50 Hz. However, WALTZ-16 at 2 kHz amplitude maintains a high correlation of 0.97 at 28.5 s, even with an offset of 2.1 kHz. In the

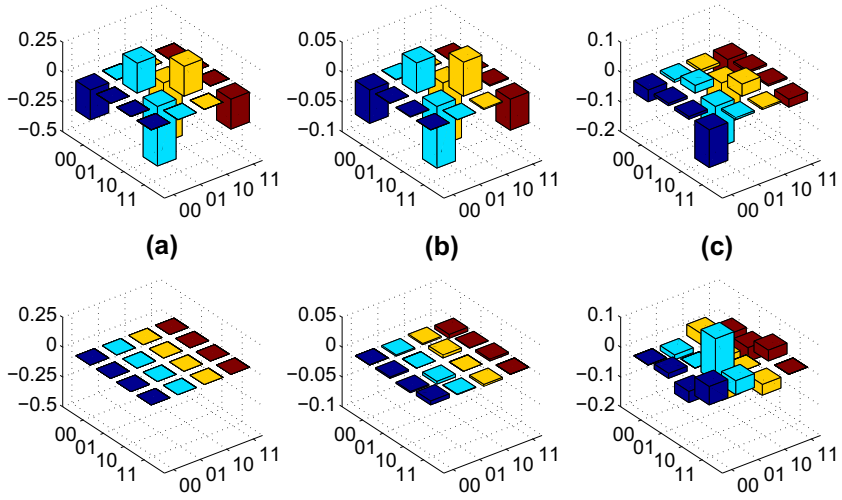


**Fig. 5.** Bar plots showing (a) traceless part $\rho_s$ of the theoretical singlet state density matrix, (b) experimental state after 15 s of WALTZ-16 spin-lock at an RF amplitude of 2 kHz, and (c) experimental state after 14 s of WALTZ-16 spin-lock at an RF amplitude of 500 Hz. The upper and lower traces correspond to the real and imaginary parts respectively. The singlet correlations in (b) and (c) are respectively 0.997 and 0.547. The density matrix in (b) shows significant decay, but still has high singlet content! The real part of the density matrix in (c) shows significant double quantum artifact.

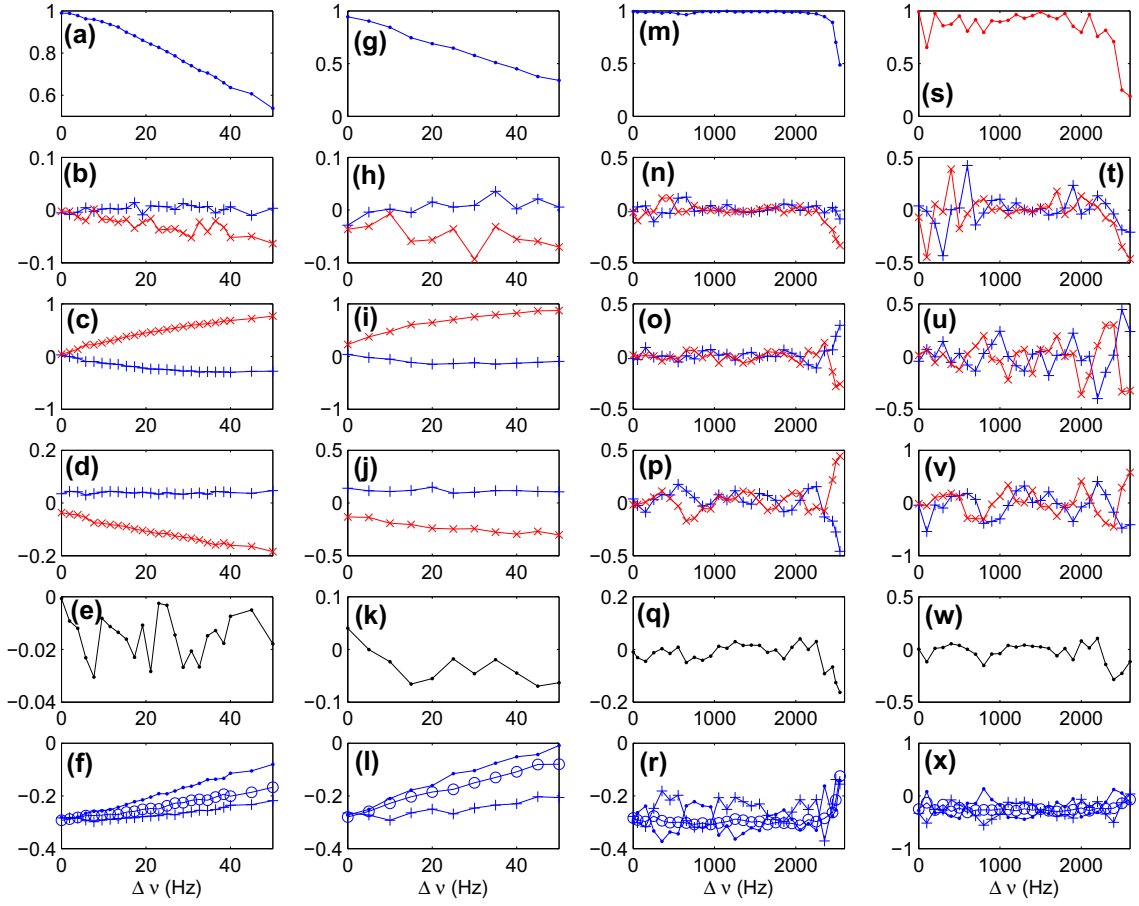


**Fig. 6.** Correlations calculated using the density matrix tomography of singlet states prepared with different spin-lock conditions: (i) CW spin-lock at 2 kHz for 15 s (a–f), (ii) CW spin-lock at 2 kHz for 28.5 s (g–l), (iii) WALTZ-16 spin-lock at 2 kHz for 15 s (m–r), and, (iv) WALTZ-16 spin-lock at 2 kHz for 28.5 s (s–x). In each case, the horizontal axis indicates the RF offset $\Delta\nu$ during the spin-lock. The offset is measured from the center of the two chemical shifts. The rows correspond to: $\langle\rho_s\rangle$ (a, g, m, and s), $\langle I_x^p\rangle$ (b, h, n, and t), $\langle I_y^p\rangle$ (c, i, o, and u), $\langle I_z^p\rangle$ (d, j, p, and v), $\langle I_+^1 I_+^2 + I_-^1 I_-^2\rangle$ (e, k, q, and w), and $c_q = \langle|T_q\rangle\langle T_q|\rangle$ (f, l, r, and x), where spin numbers $p = \{1$ (pluses), 2 (×'s)$\}$ and triplet subscripts $q = \{-1$ (dots), 0 (circles), +1 (pluses)$\}$.

case of CW spin-lock, rapid build up of y-magnetizations can be noticed with the increase of the RF offset.

## 5. Conclusions

Study of singlet state is important not only because of the interesting Physics that makes it long-lived, but also because of its potential for a number of applications. We have studied the singlet state directly and quantitatively using density matrix tomography. A new set of tomography sequences have been introduced for this purpose. The density matrix tomography provides a tool not only for characterizing various spin-lock schemes but also for understanding the spin dynamics during the spin-lock period.

The singlet state is preserved with CW spin-lock as well as with WALTZ-16 spin-lock at two different RF amplitudes: 2 kHz and 500 Hz. The results indicate that at high RF amplitudes, both CW and WALTZ-16 achieve high singlet content. An important feature of singlet state is that it gets purified by itself during the spin-lock, simply because of its longer life time compared to the spurious coherences. There exist optimum spin-lock values at which the singlet correlations are maximum. While WALTZ-16 shows significant oscillations in the singlet purity, for certain intervals of spin-lock it gives better performance than CW and holds the singlet content for longer intervals of time. The dependence of correlations with the RF offset during the spin-lock are also studied under both CW and WALTZ-16 schemes. It is found that WALTZ-16 is far superior in preserving the singlet state at large RF offsets.

## Acknowledgments

Authors gratefully acknowledge Prof. Anil Kumar, Dr. Karthik Gopalakrishnan and Dr. Avik Mitra for discussions. The use of 500 MHz NMR spectrometer at NMR Research Center, IISER-Pune is also acknowledged.

## References

[1] R.R. Ernst, G. Bodenhausen, A. Wokaun, Principles of Nuclear Magnetic Resonance in One and Two Dimensions, Oxford University Press, Oxford, 1990.
[2] M.H. Levitt, Spin Dynamics, J. Wiley and Sons Ltd., Chichester, 2002.
[3] A. Abragam, Principles of Nuclear Magnetism, Oxford University Press, 1961.
[4] M. Carravetta, O.G. Johannessen, M.H. Levitt, Beyond the T1 limit: singlet nuclear spin states in low magnetic field, Phys. Rev. Lett. 92 (2004) 153003.
[5] Carravetta, M.H. Levitt, Long-lived nuclear spin states in high-field solution NMR, J. Am. Chem. Soc. 126 (2004) 6228–6229.
[6] M. Carravetta, M.H. Levitt, Theory of long-lived nuclear spin states in solution nuclear magnetic resonance. I. Singlet states in low magnetic field, J. Chem. Phys. 122 (2005) 214505.
[7] K. Gopalakrishnan, G. Bodenhausen, Lifetimes of the singlet-states under coherent off-resonance irradiation in NMR spectroscopy, J. Magn. Reson. 182 (2006) 254–259.
[8] G. Pileio, M. Concistr, M. Carravetta, M.H. Levitt, Long-lived nuclear spin states in the solution NMR of four-spin systems, J. Magn. Reson. 182 (2006) 353–357.
[9] G. Pileio, M.H. Levitt, J-stabilization of singlet states in the solution NMR of multiple-spin systems, J. Magn. Reson. 187 (2007) 141–145.
[10] 8 E. Vinogradov, A.K. Grant, Long-lived states in solution NMR: selection rules for intramolecular dipolar relaxation in low magnetic fields, J. Magn. Reson. 188 (2007) 176–182.
[11] G. Pileio, M. Carravetta, E. Hughes, M.H. Levitt, The long-lived nuclear singlet state of 15N-nitrous oxide in solution, J. Am. Chem. Soc. 130 (2008) 12582–12583.
[12] S. Cavadini, J. Dittmer, S. Antonijevic, G. Bodenhausen, Slow diffusion by singlet state NMR spectroscopy, J. Am. Chem. Soc. 127 (2005) 15744–15748.
[13] R. Sarkar, P.R. Vasos, G. Bodenhausen, Singlet-state exchange NMR spectroscopy for the study of very slow dynamic processes, J. Am. Chem. Soc. 129 (2007) 328–334.
[14] G. Pileio, M. Carravetta, M.H. Levitt, Extremely low-frequency spectroscopy in low-field nuclear magnetic resonance, Phys. Rev. Lett. 103 (2009) 083002.
[15] A.K. Grant, E. Vinogradov, Long-lived states in solution NMR: theoretical examples in three-and four-spin systems, J. Magn. Reson. 193 (2008) 177–190.
[16] T. Jonischkeit, U. Bommerich, J. Stadler, K. Woelk, H.G. Niessen, J. Bargon, Generating long-lasting $^{1}H$ and $^{13}C$ hyperpolarization in small molecules with parahydrogen-induced polarization, J. Chem. Phys. 124 (2006) 201109.
[17] E.Y. Chekmenev, J. Hovener, V.A. Norton, K. Harris, L.S. Batchelder, P. Bhattacharya, B.D. Ross, D.P. Weitekamp, PASADENA hyperpolarization of Succinic Acid for MRI and NMR spectroscopy, J. Am. Chem. Soc. 130 (2008) 4212–4213.
[18] P.R. Vasos, A. Comment, R. Sarkar, P. Ahuja, S. Jannin, J.P. Ansermet, J.A. Konter, P. Hautle, B. van den Brandt, G. Bodenhausen, Long-lived states to sustain hyperpolarized magnetization, Proc. Natl. Acad. Sci. 106 (2009) 18469–18473.
[19] R.W. Adams, J.A. Aguilar, K.D. Atkinson, M.J. Cowley, P.I.P. Elliott, S.B. Duckett, G.G.R. Green, I.G. Khazal, J. Lopez-Serrano, D.C. Williamson, Reversible interactions with para-hydrogen enhance NMR sensitivity by polarization transfer, Science 323 (2009) 1708–1711.
[20] W.S. Warren, E. Jenista, R.T. Branca, X. Chen, Increasing hyperpolarized spin lifetimes through true singlet eigenstates, Science 323 (2009) 1711–1714.
[21] R. Sarkar, P. Ahuja, D. Moskau, P.R. Vasos, G. Bodenhausen, Extending the scope of singlet-state spectroscopy, ChemPhysChem 8 (2007) 2652–2656.
[22] G. Pileio, M.H. Levitt, Theory of long-lived nuclear spin states in solution nuclear magnetic resonance. II. Singlet spin-locking, J. Chem. Phys. 130 (2009) 214501.
[23] P. Ahuja, R. Sarkar, P.R. Vasos, G. Bodenhausen, Long-lived states in multiple-spin systems, ChemPhysChem 10 (2009) 2217–2220.
[24] I.L. Chuang, N. Gershenfeld, M.G. Kubinec, D.W. Leung, Bulk quantum computation with nuclear magnetic resonance: theory and experiment, Proc. R. Soc. London, A 454 (1998) 447–467.
[25] D. Leung, L. Vandersypen, X. Zhou, M. Sherwood, C. Yannoni, M. Kubinec, I.L. Chuang, Experimental realization of a two-bit phase damping quantum code, Phys. Rev. A 60 (1999) 1924.
[26] Ranabir Das, T.S. Mahesh, Anil Kumar, Efficient quantum state tomography for quantum information processing using a two-dimensional Fourier transform technique, Phys. Rev. A 67 (2003) 062304.
[27] G.H. Golub, C.F.V. Loan, Matrix Computations, Johns Hopkins University Press, 1996.
[28] M.H. Levitt, L. Di Bari, Steady state in magnetic resonance pulse experiments, Phys. Rev. Lett. 69 (1992) 3124.